ACS Photonics

pubs.acs.org/journal/apchd5

Article

Ultrafast Terahertz Self-Induced Absorption and Phase Modulation on a Graphene-Based Thin Film Absorber

Anastasios D. Koulouklidis,* Anna C. Tasolamprou, Spyros Doukas, Eudokia Kyriakou, M. Said Ergoktas, Christina Daskalaki, Eleftherios N. Economou, Coskun Kocabas, Elefterios Lidorikis, Maria Kafesaki, and Stelios Tzortzakis

Cite This: https://doi.org/10.1021/acsphotonics.2c00828

Read Online

ACCESS | Metrics & More | Article Recommendations | Supporting Information

ABSTRACT: Interaction of intense terahertz (THz) waves with graphene based modulation devices holds great potential for the optoelectronic applications of the future. Here, we present a thin film graphene-based THz perfect absorbing device whose absorption and phase characteristics can be modulated through THz self-actions in the subps time scale. The device consists of a single-layer graphene placed on an ionic liquid substrate, back-plated by a metallic back-reflector, with the graphene doping level mediated through electrostatic gating. We experimentally record an absorption modulation of more than 3 orders of magnitude from the initial perfect absorption state, when the device is illuminated with THz field strengths in the range of 102 to 654 kV/cm. Furthermore, an absolute phase modulation of 130° is recorded. Detailed theoretical analysis indicates that the origin of the THz nonlinear response is the THz-induced heating of the graphene's carriers that leads to a reduction of its conductivity and, consequently, to reduced absorption of the THz radiation. Our analysis also maps the temporal dynamics of the THz-induced temperature elevation of the graphene's carriers, illustrating the ultrafast, subps nature of the overall process. These results can find applications in future dynamically controlled flat optics and spatiotemporal shaping of intense THz electric fields.

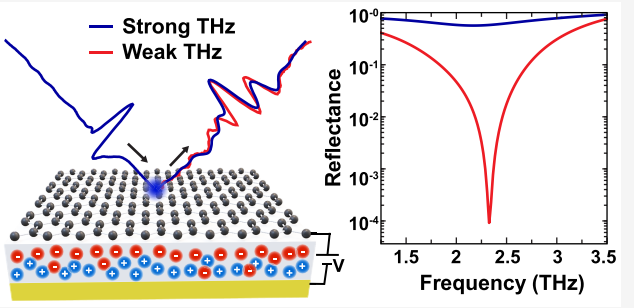

KEYWORDS: *nonlinear THz graphene, hot carriers, thermalization, terahertz self-induced modulation, graphene, perfect absorption*

INTRODUCTION

Terahertz (THz) radiation technology aims to bridge the realms of electronics and photonics, and therefore it attracts increasing attention over the last two decades. Due to their unique characteristics, that is, nonionizing nature, transparency of many nonconductive materials, and direct probing of vibrational and rotational modes in molecules, THz waves have been extensively utilized for a variety of applications, such as medical diagnostics, industrial quality control, food inspection, and many more.[1−3] Important applications refer to THz wireless communication systems, particularly within the landscape of the fast emerging 5G and 6G technologies[4,5] where THz waves promise increased bandwidths for the data demanding systems. In the quest of achieving the necessary tunabilty to efficiently undertake THz modulation, various materials and devices have been explored, such as diodes,[6] phase changing materials[7] and more.[8,9] One of the most promising such materials is graphene, whose unique mechanical and optical properties stand in the center of the research attention in recent years.[10] So far, graphene has been proposed for a plethora of optoelectronic THz components controlling both propagating and localized surface plasmons on graphene-based waveguide modulators,[11] emitters and detectors for terahertz radiation,[12,13] topological routing,[14] and metasurfaces with exotic functionalities. Additionally, graphene is expected to play a key role in space−time modulation, which further expands the wave interaction impact.[15−18]

Graphene predominantly exhibits a Drude-like response in the THz part of the spectrum, due to its easily generated and controlled free carriers. Its optical properties can be largely modulated through chemical doping and external electrostatic or magnetic fields.[19,20] Additionally, graphene optical response can be modified in an ultrafast manner; hot electrons excited by optical pulses can lead to a subps transient modulation of its conductivity.[21] Similar effects are observed under intense THz pulse excitation, where hot carrier nonlinear effects dominate the response.[22] In fact, graphene is considered to be a particularly highly nonlinear material at THz frequencies.[22]

Received: May 31, 2022

The nature of this nonlinear response has been related to the collective thermodynamic response of the background Dirac electrons under the application of intense THz fields, resulting in THz-induced carrier heating.[23] Many interesting nonlinear features of graphene have been observed, which may be further facilitated by the rapid development of high power THz sources.[24−26] Experimental studies have demonstrated the emission of THz-induced high harmonics,[27] graphene plasmon nonlinear absorption,[28] saturable absorption,[29] and the electric tunabilty of the graphene's nonlinearity.[30]

An efficient modulator involves the tunable and near unity (perfect) absorption which can be achieved in a simple Salisbury screen configuration, where a uniform graphene sheet is placed on top of a dielectric substrate, back platted by a metallic back-reflector. Such a structure has been shown to provide perfect absorption mediated by electrostatic gating.[31] Recently, we demonstrated that such a configuration can also provide ultrafast THz modulation, in the order of a few ps, when optically excited.[21] Here we demonstrate an electrically gate-tuned graphene-based Salisbury screen device, whose absorption and phase characteristics can be self-modulated when the intensity of the incident THz field is high enough to drive the graphene layer in the nonlinear regime. We record an amplitude modulation of more than 3 orders of magnitude in the resonant absorption of our device and an absolute phase modulation of 130° when the THz field strength increases from 102 to 654 kV/cm. To unveil the origin of this nonlinear response, we perform a detailed theoretical analysis based on the dynamics of single layer graphene (SLG) hot carriers,[32,33] and we attribute it to a THz-induced temperature increase of graphene carriers that is followed by a drop in the conductivity and a reduction in the THz absorption. Through our analysis, the temporal dynamics of this THz-induced temperature elevation is mapped, illustrating an ultrafast, subps response of the entire phenomenon.

EXPERIMENTAL IMPLEMENTATION

For the excitation of the graphene device, we employ a powerful THz time domain spectrometer (THz-TDS), which is based on a two-color filamentation of ultrashort laser pulses in air and operates in reflection mode.[34] This source provides ultrabroadband THz pulses (>18 THz) with peak electric field strength values up to 700 kV/cm. Figure 1a shows the incident THz electric field measured through an air-biased coherent detection (ABCD) technique[34,35] together with its corresponding power spectrum (inset of Figure 1a). The THz beam illuminates the sample at an angle of 16° with a TM (transverse magnetic) polarization. In the experiments, we have chosen electro-optic detection in a 100 μm thick gallium phosphide (GaP) ⟨110⟩ crystal, as it offers a better signal-to-noise ratio compared to the ABCD scheme. The detection crystal was optically contacted to a 2 mm thick GaP ⟨100⟩ crystal in order to avoid any Fabry−Perot spectral oscillations, extending the available temporal window to 12 ps. The strength of the THz field on the graphene sample was controlled with a pair of wire grid polarizers, and the device was characterized in the range of field strengths between 102 and 654 kV/cm. The lowest peak field strength was limited by the noise level of the detection system. Finally, water vapor absorption by the THz radiation was avoided by enclosing the whole experimental setup in a purge gas chamber.

Figure 1b presents a schematic of the graphene-based device. The THz cavity is formed by a chemical vapor deposition

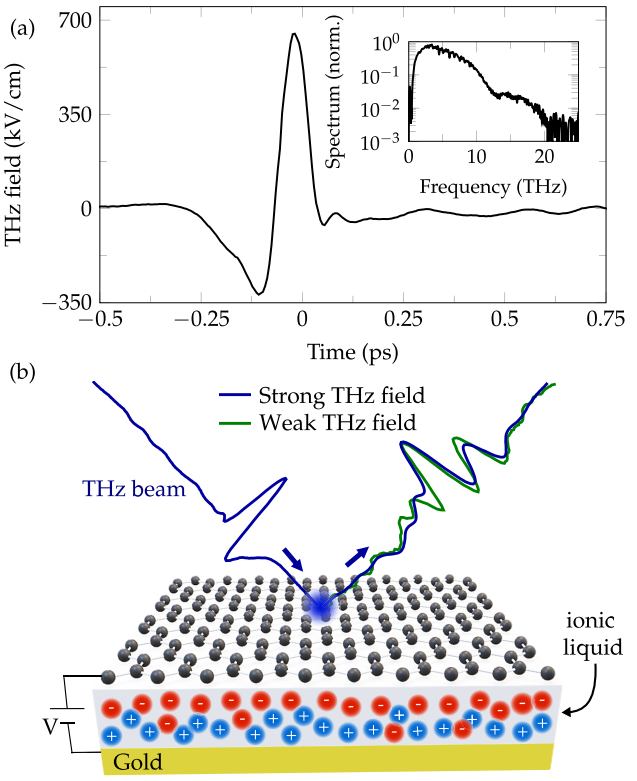

Figure 1. Schematic representation of the graphene absorber structure. The device is composed of a single-layer graphene, a membrane soaked with a room-temperature ionic liquid electrolyte of thickness d = 25 μm, and a metallic back-reflector. Fermi energy of graphene can be controlled through electrostatic gating. The THz beam illuminates the sample at an angle of 16°.

(CVD) grown single layer graphene as the top electrode, a 25 μm thick porous polyethylene membrane containing a room temperature ionic liquid electrolyte (DEME-TFSI)[31] as cavity layer, and a gold electrode as a back reflector.[18,31] The Fermi energy of graphene can be fine-tuned through an external electric gating between the graphene layer and the grounded back gold electrode. When no voltage is applied to the device the graphene layer is positively doped due to the nature of growth and transfer processes.[18,31] The doping level is enough to satisfy the coherent perfect absorption conditions[21,31] without any electrostatic gating (0 V).

Figure 2a shows normalized measured THz electric fields for the cases of the lowest and highest available THz field strengths. Due to the high bandwidth of our THz-TDS system we are able to resolve both reflective interfaces of the device that manifest themselves as two distinct peaks on the THz field: one at −0.25 ps originating from the reflection of the THz pulse on the graphene layer and one at 0 ps that originates from the gold back reflector (see Figure 2b). From Figure 2a we see that, as the THz field strength increases, we record a drop on the THz reflectivity of the graphene layer compared to the one from the gold back reflector. This indicates a THz-induced negative photoconductivity on the graphene layer. Additionally, we observe an overall modulation of the THz electric field shape indicating also a modulation of the THz field phase.

The nonlinear behavior is depicted more clearly in the electrical response of the graphene layer in the presence of the external electrostatic gating. Therefore, we measured the THz

https://doi.org/10.1021/acsphotonics.2c00828
ACS Photonics XXXX, XXX, XXX−XXX

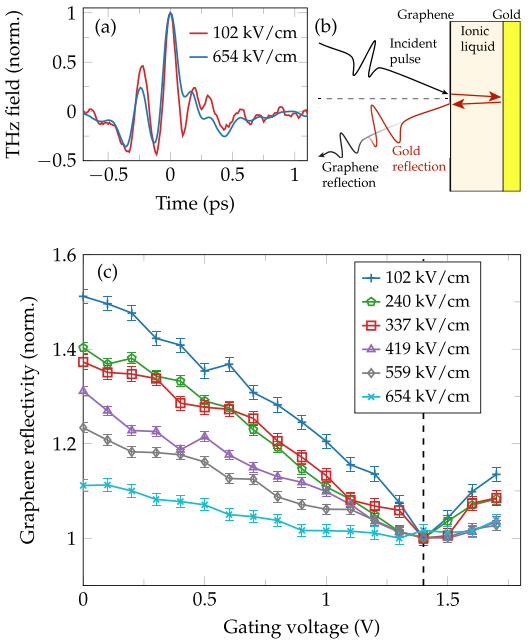

Figure 2. (a) Normalized THz electric fields in the case of 102 (red curve) and 654 kV/cm (blue curve). (b) Schematic representation of the formation of the THz field shape after its reflection on the graphene device. (c) THz reflectivity of the gated graphene layer alone, as a function of both the THz field strength and the Fermi energy level, defined by the gating voltage. All curves are normalized to the response at the CNP of graphene indicated with the dashed line at 1.4 V.

reflectivity variation only of the graphene layer by recording the peak of the THz electric field that corresponds to the graphene layer (time = −0.25 ps) as a function of the gate voltage. Figure 2c shows the reflectivity variation for different incident peak electric fields in the range of 102 to 654 kV/cm. All curves are normalized to the charge neutral point (CNP) of graphene (dashed line at 1.4 V) defined as the gating voltage, at which the graphene resistance becomes maximum and, consequently, the THz reflectivity becomes minimum due to the increased transmission. We observe that the graphene THz reflectivity induced by the gating voltage depends nonlinearly on the THz field strength. At low THz fields, we record a modulation of the THz reflectivity up to 50% at 0 V. However, at high THz field strengths, this modulation drops to 10%. All the following measurements were performed at 0 V, where the maximum modulation on the graphene reflectivity was observed.

The aforementioned THz-induced photoconductivity modulation, is expected to impact the absorption and phase characteristics of the whole device. The reflectance, normalized to the reflectance at the CNP, and associated phase spectra of the device for varying THz field strengths, are shown in Figure 3a and b, respectively. At low THz field strengths our device operates at the perfect absorption conditions, presenting a resonance at frequency f = 2.33 THz, defined by the device design and the angle of incidence of the THz radiation. The reflectance of the device at this frequency drops down to 9.2 × 10^{-5}. However, as the THz field strength increases, the perfect absorption conditions are disrupted and the reflectance of the device increases to 0.57 for the maximum available THz field strength. This corresponds to a THz-induced absorption modulation of more than 3 orders of magnitude. Moreover, a slight red shift of the resonance with increasing THz field strength is observed. In Figure 3b we observe also a significant phase modulation at frequencies around the resonance (region between dashed lines in Figure 3b). We recorded an absolute THz-induced phase modulation of 130°. This large phase modulation is responsible for the THz pulse reshaping (see Figure 2a) when the THz field strength scales up. In order to exclude any nonlinearities induced by the intense THz fields on the ionic liquid substrate, we investigated separately a similar sample without the graphene layer, and we did not observe any THz nonlinear response.

DISCUSSION AND INTERPRETATION

In order to understand the origin of the observed nonlinear response, we performed a detailed modeling of the graphene's response to THz excitation. Figure 4 shows a schematic representation of this response. After the absorption of the incoming THz radiation, graphene carriers thermalize in an ultrafast (∼20 fs)[36,37] time scale. Heat dissipation occurs in a much slower (∼ps)[32,38] time scale via emission of optical phonons[38,39] and disorder-assisted supercollisions.[38,40,41] This leads to heat accumulation in the graphene carrier bath, raising the electronic temperature T_e. The elevated T_e results in a

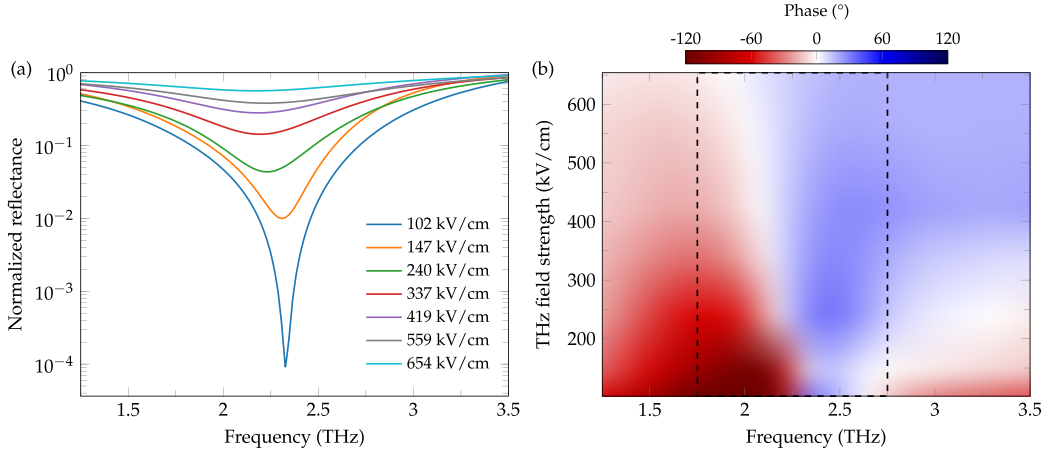

Figure 3. Experimentally measured reflectance (a) and phase (b) spectra for the cavity structure presented in Figure 1, for various values of THz field strength in the range of 102−654 kV/cm. All spectra are normalized at the CNP.

https://doi.org/10.1021/acsphotonics.2c00828
ACS Photonics XXXX, XXX, XXX−XXX

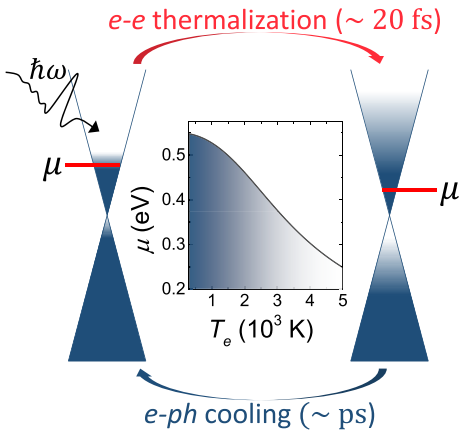

Figure 4. Schematic representation of graphene carriers upon heating, following THz excitation. Chemical potential (red line) and carrier distribution are sketched at room temperature (left) and at $T_e \gg 300$ K (right). The middle graph plots the reducing graphene chemical potential with increasing T_e as a consequence of carrier conservation.

reduced graphene chemical potential due to net carrier density conservation (i.e., $n_e(\mu, T_e) - n_h(\mu, T_e) = \text{const}$, where $n_e(\mu, T_e)$ and $n_h(\mu, T_e)$ are the graphene electron and hole densities, respectively, and μ is the graphene chemical potential[32]), and a broadened Fermi–Dirac distribution of graphene carriers. This reduces the intraband transitions, as explicitly evaluated by the Kubo formula,[32] leading to a reduced intraband conductivity,[23,42] and thus to a reduced THz absorbance of graphene.[32]

In order to quantitatively describe the above, graphene carrier and temperature dynamics are time integrated using a fourth-order Runge–Kutta method (4RK).[32] To do so we assume a two-temperature model[32,43]

$$c_e \frac{\partial T_e}{\partial t} = \alpha_{SLG}(\omega, T_e) P_{in}(\omega, t) - J_{e\text{-}ph}(T_e, T_l) \quad (1)$$

$$c_l \frac{\partial T_l}{\partial t} = J_{e\text{-}ph}(T_e, T_l) - \Gamma_{SLG\text{-}sub}(T_l - T_{sub}) \quad (2)$$

where c_e and c_l are the electronic and lattice graphene thermal capacities,[32,44] T_e and T_l are the graphene carrier and lattice temperatures, which are generally different,[32,43] $\alpha_{SLG}(\omega, T_e)$ is the graphene absorption, which depends on T_e and light frequency ω, $P_{in}(\omega, t)$ is the input power density of the THz source, $J_{e\text{-}ph}(T_e, T_l)$ is the thermal current density from the electron to the phonon bath, $\Gamma_{SLG\text{-}sub} \approx 20$ MW m^{-2} K^{-1} is the cooling rate of graphene lattice into the substrate,[32] and T_{sub} is the substrate temperature, assumed for simplicity to be fixed at 300 K. For the input power density, we assume a Gaussian pulse profile, that is, $P_{in}(\omega, t) = P(\omega) \exp(-B(t/\tau_w)^2)$, with $B = 4\ln(2)$, $\tau_w \approx 150$ fs is the full width at half-maximum of the pulse, and $P(\omega)$ is the spectral profile of the input pulse. The spectral profile $P(\omega)$ is determined experimentally (see inset of Figure 1a) and is normalized so that $\int_0^\infty P_{in}(\omega, t)dt$ yields the pulse fluence measured in the experiment. Terms c_e, c_l, and $J_{e\text{-}ph}(T_e, T_l)$ are calculated as described in ref 32. For $J_{e\text{-}ph}(T_e, T_l)$, we explicitly account[32] for electron–optical phonon scattering[32,38,39] as well as supercollision scattering.[32,40,41] For the latter, we assume short-range scatterers with a mean free path l,[32,40,41] yielding a supercollision thermal current density scaling with l^{-1}. THz light absorption in graphene is governed by intraband absorption, described by the frequency-dependent intraband graphene conductivity:[23,32,45]

$$\sigma(\omega) = \frac{ie^2}{\pi\hbar^2} \int_0^\infty dE \frac{E}{\omega + i\tau^{-1}(E)} \left[\frac{\partial f_{FD}(-E; \mu_{SLG}, T_e)}{\partial E} - \frac{\partial f_{FD}(E; \mu_{SLG}, T_e)}{\partial E} \right] \quad (3)$$

where $f_{FD}(E; \mu_{SLG})$ is the Fermi–Dirac distribution and $\tau(E)$ the energy-dependent momentum scattering time.[23] The latter is modeled assuming unscreened long-range scattering in Coulomb impurities, that is, $\tau(\epsilon) = \gamma\epsilon$, as expected in CVD-grown graphene,[22,23,42,46] where $\gamma = n_i\pi^2 e^4/\hbar\epsilon_{sub}^2$, with ϵ_{sub} being the substrate dielectric constant, depends on impurity concentration n_i[46] and will be treated as a free parameter. A full microscopic description can be used to account for effects of screening[47] and electron–phonon scattering[48] on the relaxation time. However, at the high Fermi levels ($\geq$0.2 eV) and substrate supported graphene with low ($<10^4$ cm^2/(V s)) mobility used in our study, it is found to result in an overall linear dependence with carrier energy.[42,49] This linear scaling has also been successfully implemented in describing conductivity changes upon carrier heating.[22,23] Thus, to avoid the addition of extra free parameters (which could lead to overfitting the experimental data) we follow the simplified linear scaling model of the unscreened case and fit the

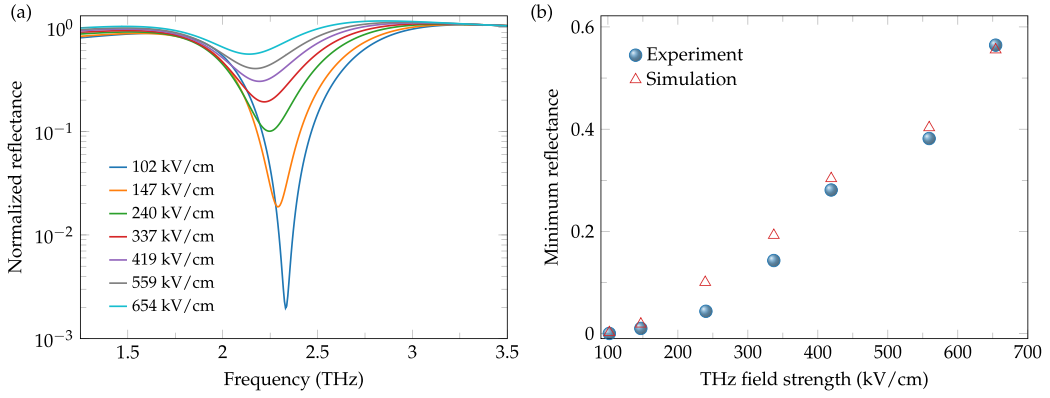

Figure 5. (a) Reflectance spectra, for different THz field strengths for the cavity structure presented in Figure 1, as calculated from our model using $E_{F,SLG} = 0.56$ eV, $l = 75$ nm, and $\gamma = 170$ fs/eV. All spectra are normalized at the CNP. (b) Experimental and calculated minimum reflectance of the proposed device as a function of THz field strength.

https://doi.org/10.1021/acsphotonics.2c00828
ACS Photonics XXXX, XXX, XXX−XXX

proportionality constant γ and graphene E_F to the experimental results. Using eq 3 for graphene Drude conductivity, we calculate the dielectric function from which graphene's absorption $\alpha_{SLG}(\omega, T_e)$ can be determined.[32] The substrate's contribution to the optical response is determined by fitting the device's reflectivity, prior to graphene placement, assuming a 25 μm substrate thickness. We fit the substrate's dielectric response using a single Lorentz oscillator.[50] The extracted Lorentz parameters are $\epsilon_\infty = 3.29$, $\Delta\epsilon = 1.45$ eV, $\hbar\Omega = 5.42$ meV, and $\hbar\Gamma = 9.28$ meV, where ϵ_∞ is the value of the dielectric function at infinite frequency, $\Delta\epsilon$ is the oscillator strength, $\hbar\Omega$ is the transition frequency, and $\hbar\Gamma$ is the decay rate of the Lorentz term. The overall optical response of the proposed device, including the contributions of the substrate and the back-mirror, is calculated by employing the Fresnel equations using the transfer matrix method (TMM). Finally, the reflection spectrum of the device is calculated as

$$R(\omega) = \frac{\int_0^\infty P_{in}(\omega, t)R(\omega, t)\ dt}{\int_0^\infty P_{in}(\omega, t)\ dt} \quad (4)$$

where $R(\omega, t)$ is the time-dependent reflection resulting from TMM, which includes all the definitions of eqs 1−3, self-consistently updated during the time integration within the 4RK scheme.[32]

Therefore, the only free parameters for our model are the graphene Fermi level $E_{F,SLG}$, the proportionality constant γ for long-range Coulomb scattering,[22,23] and the mean-free path for supercollision scattering l.[32,40,41] We scan a wide range of these three parameters in order to minimize the deviations between our calculations and the experimental measurements. Good quantitative agreement between calculations and experiment (see Figure 5b) is found for $E_{F,SLG} \approx 0.56$ eV, $l \approx 75$ nm, and $\gamma \approx 170$ fs/eV. The latter yields a momentum relaxation time of $\tau \approx 95$ fs at room temperature, which corresponds to a carrier mobility of $\mu_q \approx 1700$ cm^2 V^{-1} s^{-1}. The values for $E_{F,SLG}$ and τ extracted from our model match very well to previous reports in similar devices.[18,31] Moreover, the supercollision mean free path is within the range of previous reported values[40,41] for graphene on a dielectric substrate. These demonstrate the usefulness of our model as a reliable tool for extracting graphene's parameters using as input the experimental optical measurements.

Figure 5a shows the reflectance spectra, for different THz field strengths, as calculated from our model. The above spectra are acquired after normalization of the reflectance at zero bias to the reflectance at CNP (1.4 V bias). For this normalization we assumed $E_{F,SLG} \approx 200$ meV at CNP. The above value was determined after fitting the calculated spectra to experimental measurements under 1.4 V bias and is in line with previously reported values of graphene residual doping on ionic liquid substrates.[18,31,51] We observe a similar behavior with the experimental findings (see Figure 3). As the THz field increases, so does the calculated reflectance, presenting also the characteristic red shift of the resonance observed in the experiment. This absorption resonance is due to critical coupling of light[19] into the Fabry−Perot cavity formed by the graphene reflector and the back mirror and is sharper in theory compared to experiment. The latter can be attributed to inhomogeneous broadening originating from substrate thickness and graphene doping fluctuations across the measurement spot size. At frequencies far from resonance, on the other hand, an antiresonance is expected, where the total reflection of the graphene−mirror system is larger than the reflection at CNP (where graphene is nonreflecting) and thus the normalized reflectance reaches above unity. We note that this behavior is observed in the theoretical spectra but not in the experimental spectra, which is most likely due to the aforementioned inhomogeneous broadening. In Figure 5b we plot the minimum reflectance, as a function of peak THz field strength, alongside the experimental results. The final results for the on resonance reflectance modulation shows a good agreement between theory and experiment.

It is evident that a higher THz field strength yields a larger overall reflectance. As discussed, this can be attributed to the heating of graphene carriers and the subsequent lowering of the graphene chemical potential and the reduction of its intraband conductivity. Therefore, graphene absorbance is reduced, and as a result, the reflectance of the incoming THz radiation increases. The temporal evolution of the differential reflectance at resonant frequency during THz excitation can be found in the Supporting Information. There, we also extract a relationship between peak relative reflectance increase at resonance as a function of incoming THz field strength, yielding $\Delta R_{max} \approx \beta E_{max}$, with $\beta = 3.4 \times 10^{-4}$ cm/kV.

Our theoretical framework allows one to gain insight into the carrier temporal dynamics during THz excitation. Figure 6a shows the temporal evolution of carrier temperature, during, and shortly after the THz excitation. In Figure 6b we plot the respective temporal evolution of the real part of intraband conductivity (which is directly proportional to THz graphene absorbance) at the resonant frequency. This elucidates how the near instantaneous thermalization of graphene carriers, in combination with their restarted cooling, leads to vanishing conductivity at higher THz field strengths. The latter is the source of the nonlinear absorption modulation observed in this work. Furthermore, we observe that the overall phenomenon occurs on the subps time scale, illustrating the ultrafast nature of the observed modulation. The temporal evolution of the differential conductivity is also included in the Supporting Information, along with the photoconductivity minima relation

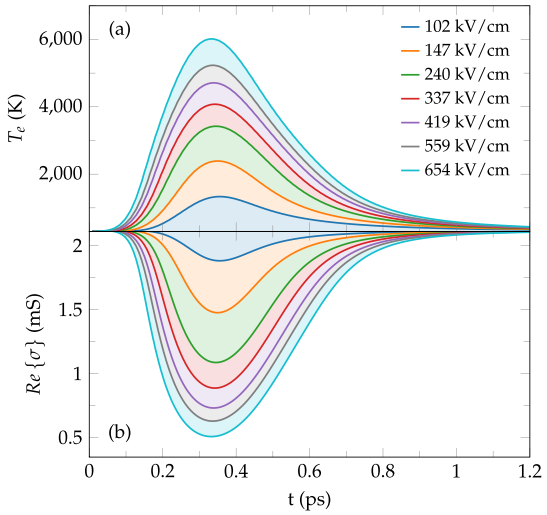

Figure 6. Calculated temporal evolution of (a) graphene carriers' temperature and (b) real part of intraband conductivity at the resonant frequency.

https://doi.org/10.1021/acsphotonics.2c00828
ACS Photonics XXXX, XXX, XXX−XXX

on the excitation THz field strength, yielding $\sigma_{min} = 0.035E_{max}^{-\alpha}$, with $\alpha = 0.63$.

CONCLUSION

We have demonstrated that, under the excitation of intense THz pulses, a graphene-based Salisbury screen perfect absorbing device can be self-modulated in terms of its absorption properties. In our experiments, we observed an absorption modulation of more than 3 orders of magnitude at 2.33 THz and an absolute phase modulation of 130° when the THz field strength scaled from 102 up to 654 kV/cm. Our detailed theoretical analysis based on the dynamics of the THz-induced hot carriers in a single layer graphene, shed light on the origin of the observed nonlinear response of the device: the irradiation of intense THz fields, results in heating of the graphene's carriers and a subsequent decrease of its chemical potential and intraband conductivity. The carrier temporal dynamics during THz excitation, obtained through our split-time algorithm, reveals the ultrafast nature of the nonlinear response since the entire phenomenon lasts less than a picosecond. These results demonstrate a new mechanism of modulating the absorption and phase properties of graphene-based perfect absorbing devices, that of THz self-actions. Such devices could find applications in future dynamically modulated flat optics devices. Additionally, devices based on our work can serve for the custom beam and pulse shaping of intense THz sources.

ASSOCIATED CONTENT

Supporting Information

The Supporting Information is available free of charge at https://pubs.acs.org/doi/10.1021/acsphotonics.2c00828.

THz nonlinearity dependence on excitation field strength (PDF)

AUTHOR INFORMATION

Corresponding Author

Anastasios D. Koulouklidis − *Institute of Electronic Structure and Laser, Heraklion, Crete 71110, Greece;* orcid.org/0000-0003-4191-0089; Email: tasoskoul@iesl.forth.gr

Authors

Anna C. Tasolamprou − *Institute of Electronic Structure and Laser, Heraklion, Crete 71110, Greece;* orcid.org/0000-0003-4652-5470

Spyros Doukas − *Department of Materials Science and Engineering, University of Ioannina, Ioannina 45110, Greece;* orcid.org/0000-0003-3903-4569

Eudokia Kyriakou − *Institute of Electronic Structure and Laser, Heraklion, Crete 71110, Greece; Department of Materials Science and Technology, University of Crete, Heraklion, Crete 70013, Greece*

M. Said Ergoktas − *Department of Materials, University of Manchester, Manchester M13 9PL, United Kingdom; National Graphene Institute, University of Manchester, Manchester M13 9PL, United Kingdom;* orcid.org/0000-0002-8749-8571

Christina Daskalaki − *Institute of Electronic Structure and Laser, Heraklion, Crete 71110, Greece*

Eleftherios N. Economou − *Institute of Electronic Structure and Laser, Heraklion, Crete 71110, Greece; Department of Physics, University of Crete, Heraklion, Crete 70013, Greece*

Coskun Kocabas − *Department of Materials, University of Manchester, Manchester M13 9PL, United Kingdom; National Graphene Institute and Henry Royce Institute for Advanced Materials, University of Manchester, Manchester M13 9PL, United Kingdom;* orcid.org/0000-0003-0831-5552

Elefterios Lidorikis − *Department of Materials Science and Engineering, University of Ioannina, Ioannina 45110, Greece; Institute of Materials Science and Computing, University Research Center of Ioannina (URCI), Ioannina 45110, Greece;* orcid.org/0000-0002-9552-9366

Maria Kafesaki − *Institute of Electronic Structure and Laser, Heraklion, Crete 71110, Greece; Department of Materials Science and Technology, University of Crete, Heraklion, Crete 70013, Greece*

Stelios Tzortzakis − *Institute of Electronic Structure and Laser, Heraklion, Crete 71110, Greece; Department of Materials Science and Technology, University of Crete, Heraklion, Crete 70013, Greece; Science Program, Texas A&M University at Qatar, Doha, Qatar*

Complete contact information is available at: https://pubs.acs.org/10.1021/acsphotonics.2c00828

Funding

This work was supported by the European Union's Horizon 2020 research and innovation program under Grant Agreement No. 881603 Graphene Flagship for Core3 and the "ENTERS" research project funded by the Hellenic Foundation for Research and Innovation (HFRI).

Notes

The authors declare no competing financial interest.

REFERENCES

(1) Tonouchi, M. Cutting-edge terahertz technology. *Nat. Photonics* **2007**, *1*, 97−105.

(2) Yang, X.; Zhao, X.; Yang, K.; Liu, Y.; Liu, Y.; Fu, W.; Luo, Y. Biomedical Applications of Terahertz Spectroscopy and Imaging. *Trends Biotechnol.* **2016**, *34*, 810−824.

(3) Wang, Q.; Xie, L.; Ying, Y. Overview of imaging methods based on terahertz time-domain spectroscopy. *Appl. Spectrosc. Rev.* **2022**, *57*, 249−264.

(4) Akyildiz, I. F.; Kak, A.; Nie, S. 6G and Beyond: The Future of Wireless Communications Systems. *IEEE Access* **2020**, *8*, 133995−134030.

(5) Liaskos, C.; Tsioliaridou, A.; Ioannidis, S.; Pitsillides, A.; Akyildiz, I. F. Realizing Ambient Backscatter Communications with Intelligent Surfaces in 6G Wireless Systems. *IEEE Wireless Communications* **2022**, *29*, 178−185.

(6) Mehdi, I.; Siles, J. V.; Lee, C.; Schlecht, E. THz Diode Technology: Status, Prospects, and Applications. *Proceedings of the IEEE* **2017**, *105*, 990−1007.

(7) Jeong, Y.-G.; Bahk, Y.-M.; Kim, D.-S. Dynamic Terahertz Plasmonics Enabled by Phase-Change Materials. *Advanced Optical Materials* **2020**, *8*, 1900548.

(8) Rahm, M.; Li, J.-S.; Padilla, W. J. THz Wave Modulators: A Brief Review on Different Modulation Techniques. *J. Infrared Milli Terahz Waves* **2013**, *34*, 1−27.

(9) Degl'Innocenti, R.; Lin, H.; Navarro-Cía, M. Recent Progress in Terahertz Metamaterial Modulators. *Nanophotonics* **2022**, *11*, 1485−1514.

(10) Ferrari, A.; et al. Science and technology roadmap for graphene, related two-dimensional crystals, and hybrid systems. *Nanoscale* **2015**, *7*, 4598−4810.

(11) Mittendorff, M.; Li, S.; Murphy, T. E. Graphene-Based Waveguide-Integrated Terahertz Modulator. *ACS Photonics* **2017**, *4*, 316−321.
(12) Castilla, S.; Terrés, B.; Autore, M.; Viti, L.; Li, J.; Nikitin, A. Y.; Vangelidis, I.; Watanabe, K.; Taniguchi, T.; Lidorikis, E.; Vitiello, M. S.; Hillenbrand, R.; Tielrooij, K.-J.; Koppens, F. H. Fast and Sensitive Terahertz Detection Using an Antenna-Integrated Graphene pn Junction. *Nano Lett.* **2019**, *19*, 2765−2773.
(13) Tong, J.; Muthee, M.; Chen, S.-Y.; Yngvesson, S.; Yan, J. Antenna Enhanced Graphene THz Emitter and Detector. *Nano Lett.* **2015**, *15*, 5295−5301.
(14) Jin, D.; Christensen, T.; Soljačić, M.; Fang, N. X.; Lu, L.; Zhang, X. Infrared Topological Plasmons in Graphene. *Phys. Rev. Lett.* **2017**, *118*, 245301.
(15) Pendry, J.; Huidobro, P.; Silveirinha, M.; Galiffi, E. Crossing the light line. *Nanophotonics* **2021**, *11*, 161−167.
(16) Shaltout, A.; Shalaev, V.; Brongersma, M. Spatiotemporal light control with active metasurfaces. *Science* **2019**, *364*, No. eaat3100.
(17) Tirole, R.; Galiffi, E.; Dranczewski, J.; Attavar, T.; Tilmann, B.; Wang, Y.-T.; Huidobro, P. A.; Alú, A.; Pendry, J. B.; Maier, S. A.; Vezzoli, S.; Sapienza, R. Saturable time-varying mirror based on an ENZ material. https://arxiv.org/abs/2202.05937 (accessed 2022−08−01).
(18) Malevich, Y.; Ergoktas, M. S.; Bakan, G.; Steiner, P.; Kocabas, C. Video-Speed Graphene Modulator Arrays for Terahertz Imaging Applications. *ACS Photonics* **2020**, *7*, 2374−2380.
(19) Doukas, S.; Chatzilari, A.; Dagkli, A.; Papagiannopoulos, A.; Lidorikis, E. Deep and fast free-space electro-absorption modulation in a mobility-independent graphene-loaded Bragg resonator. *Appl. Phys. Lett.* **2018**, *113*, 011102.
(20) Guo, Q.; Li, C.; Deng, B.; Yuan, S.; Guinea, F.; Xia, F. Infrared Nanophotonics Based on Graphene Plasmonics. *ACS Photonics* **2017**, *4*, 2989−2999.
(21) Tasolamprou, A. C.; Koulouklidis, A. D.; Daskalaki, C.; Mavidis, C. P.; Kenanakis, G.; Deligeorgis, G.; Viskadourakis, Z.; Kuzhir, P.; Tzortzakis, S.; Kafesaki, M.; Economou, E. N.; Soukoulis, C. M. Experimental Demonstration of Ultrafast THz Modulation in a Graphene-Based Thin Film Absorber through Negative Photoinduced Conductivity. *ACS Photonics* **2019**, *6*, 720−727.
(22) Hafez, H. A.; Kovalev, S.; Tielrooij, K.-J.; Bonn, M.; Gensch, M.; Turchinovich, D. Terahertz nonlinear optics of graphene: from saturable absorption to high-harmonics generation. *Advanced Optical Materials* **2020**, *8*, 1900771.
(23) Mics, Z.; Tielrooij, K.-J.; Parvez, K.; Jensen, S. A.; Ivanov, I.; Feng, X.; Müllen, K.; Bonn, M.; Turchinovich, D. Thermodynamic picture of ultrafast charge transport in graphene. *Nat. Commun.* **2015**, *6*, 1−7.
(24) Koulouklidis, A. D.; Gollner, C.; Shumakova, V.; Fedorov, V. Y.; Pugžlys, A.; Baltuška, A.; Tzortzakis, S. Observation of extremely efficient terahertz generation from mid-infrared two-color laser filaments. *Nat. Commun.* **2020**, *11*, 292.
(25) Shalaby, M.; Hauri, C. P. Demonstration of a low-frequency three-dimensional terahertz bullet with extreme brightness. *Nat. Commun.* **2015**, *6*, 5976.
(26) Dey, I.; Jana, K.; Fedorov, V. Y.; Koulouklidis, A. D.; Mondal, A.; Shaikh, M.; Sarkar, D.; Lad, A. D.; Tzortzakis, S.; Couairon, A.; Kumar, G. R. Highly efficient broadband terahertz generation from ultrashort laser filamentation in liquids. *Nat. Commun.* **2017**, *8*, 1184.
(27) Hafez, H.; et al. Extremely efficient terahertz high-harmonic generation in graphene by hot Dirac fermions. *Nature* **2018**, *561*, 507−511.
(28) Jadidi, M. M.; König-Otto, J. C.; Winnerl, S.; Sushkov, A. B.; Drew, H. D.; Murphy, T. E.; Mittendorff, M. Nonlinear Terahertz Absorption of Graphene Plasmons. *Nano Lett.* **2016**, *16*, 2734−2738.
(29) Bianchi, V.; Carey, T.; Viti, L.; Li, L.; Linfield, E.; Davies, A.; Tredicucci, A.; Yoon, D.; Karagiannidis, P.; Lombardi, L.; Tomarchio, F.; Ferrari, A.; Torrisi, F.; Vitiello, M. Terahertz saturable absorbers from liquid phase exfoliation of graphite. *Nat. Commun.* **2017**, *8*, 15763.
(30) Kovalev, S.; et al. Electrical tunability of terahertz nonlinearity in graphene. *Science Advances* **2021**, *7*, No. eabf9809.
(31) Kakenov, N.; Balci, O.; Takan, T.; Ozkan, V. A.; Altan, H.; Kocabas, C. Observation of Gate-Tunable Coherent Perfect Absorption of Terahertz Radiation in Graphene. *ACS Photonics* **2016**, *3*, 1531−1535.
(32) Doukas, S.; Mensz, P.; Myoung, N.; Ferrari, A. C.; Goykhman, I.; Lidorikis, E. Thermionic graphene/silicon Schottky infrared photodetectors. *Phys. Rev. B* **2022**, *105*, 115417.
(33) Mics, Z.; Tielrooij, K.-J.; Parvez, K.; Jensen, S.; Ivanov, I.; Feng, X.; Müllen, K.; Bonn, M.; Turchinovich, D. Thermodynamic picture of ultrafast charge transport in graphene. *Nat. Commun.* **2015**, *6*, 7655.
(34) Koulouklidis, A. D.; Fedorov, V. Y.; Tzortzakis, S. Spectral bandwidth scaling laws and reconstruction of THz wave packets generated from two-color laser plasma filaments. *Phys. Rev. A* **2016**, *93*, 033844.
(35) Karpowicz, N.; Dai, J.; Lu, X.; Chen, Y.; Yamaguchi, M.; Zhao, H.; Zhang, X.-C.; Zhang, L.; Zhang, C.; Price-Gallagher, M.; Fletcher, C.; Mamer, O.; Lesimple, A.; Johnson, K. Coherent heterodyne time-domain spectrometry covering the entire "terahertz gap. *Appl. Phys. Lett.* **2008**, *92*, 011131.
(36) Tomadin, A.; Brida, D.; Cerullo, G.; Ferrari, A. C.; Polini, M. Nonequilibrium dynamics of photoexcited electrons in graphene: Collinear scattering, Auger processes, and the impact of screening. *Phys. Rev. B* **2013**, *88*, 035430.
(37) Brida, D.; Tomadin, A.; Manzoni, C.; Kim, Y. J.; Lombardo, A.; Milana, S.; Nair, R. R.; Novoselov, K. S.; Ferrari, A. C.; Cerullo, G.; Polini, M. Ultrafast collinear scattering and carrier multiplication in graphene. *Nat. Commun.* **2013**, *4*, 1−9.
(38) Pogna, E. A.; Jia, X.; Principi, A.; Block, A.; Banszerus, L.; Zhang, J.; Liu, X.; Sohier, T.; Forti, S.; Soundarapandian, K.; et al. Hot-Carrier Cooling in High-Quality Graphene Is Intrinsically Limited by Optical Phonons. *ACS Nano* **2021**, *15*, 11285−11295.
(39) Viljas, J.; Heikkilä, T. Electron-phonon heat transfer in monolayer and bilayer graphene. *Phys. Rev. B* **2010**, *81*, 245404.
(40) Song, J. C.; Reizer, M. Y.; Levitov, L. S. Disorder-assisted electron-phonon scattering and cooling pathways in graphene. *Physical review letters* **2012**, *109*, 106602.
(41) Song, J. C.; Levitov, L. S. Energy flows in graphene: hot carrier dynamics and cooling. *J. Phys.: Condens. Matter* **2015**, *27*, 164201.
(42) Tielrooij, K.-J.; Song, J.; Jensen, S. A.; Centeno, A.; Pesquera, A.; Zurutuza Elorza, A.; Bonn, M.; Levitov, L.; Koppens, F. Photoexcitation cascade and multiple hot-carrier generation in graphene. *Nat. Phys.* **2013**, *9*, 248−252.
(43) Massicotte, M.; Schmidt, P.; Vialla, F.; Watanabe, K.; Taniguchi, T.; Tielrooij, K.-J.; Koppens, F. H. Photo-thermionic effect in vertical graphene heterostructures. *Nat. Commun.* **2016**, *7*, 1−7.
(44) Pop, E.; Varshney, V.; Roy, A. K. Thermal properties of graphene: Fundamentals and applications. *MRS Bull.* **2012**, *37*, 1273−1281.
(45) Pistore, V.; Balci, O.; Zhang, J.; Schinde, S. M.; Meersha, A.; Ferrari, A. C.; Vitiello, M. S. Mapping the Complex Refractive Index of Single Layer Graphene on Semiconductor or Polymeric Substrates at Terahertz Frequencies. *2D Materials* **2022**, *9*, 025018.
(46) Das Sarma, S.; Hwang, E. H. Density-dependent electrical conductivity in suspended graphene: Approaching the Dirac point in transport. *Phys. Rev. B* **2013**, *87*, 035415.
(47) Tomadin, A.; Hornett, S. M.; Wang, H. I.; Alexeev, E. M.; Candini, A.; Coletti, C.; Turchinovich, D.; Klaui, M.; Bonn, M.; Koppens, F. H. L.; Hendry, E.; Polini, M.; Tielrooij, K.-J. The ultrafast dynamics and conductivity of photoexcited graphene at different Fermi energies. *Science advances* **2018**, *4*, No. eaar5313.
(48) Hwang, E. H.; Das Sarma, S. Acoustic phonon scattering limited carrier mobility in two-dimensional extrinsic graphene. *Phys. Rev. B* **2008**, *77*, 115449.

https://doi.org/10.1021/acsphotonics.2c00828
ACS Photonics XXXX, XXX, XXX−XXX

(49) Massicotte, M.; Soavi, G.; Principi, A.; Tielrooij, K.-J. Hot carriers in graphene−fundamentals and applications. *Nanoscale* **2021**, *13*, 8376−8411.
(50) Schedin, F.; Lidorikis, E.; Lombardo, A.; Kravets, V. G.; Geim, A. K.; Grigorenko, A. N.; Novoselov, K. S.; Ferrari, A. C. Surface-Enhanced Raman Spectroscopy of Graphene. *ACS Nano* **2010**, *4*, 5617−5626.
(51) Pogna, E. A.; Tomadin, A.; Balci, O.; Soavi, G.; Paradisanos, I.; Guizzardi, M.; Pedrinazzi, P.; Mignuzzi, S.; Tielrooij, K.-J.; Polini, M.; et al. Electrically Tunable Nonequilibrium Optical Response of Graphene. *ACS Nano* **2022**, *16*, 3613−3624.

https://doi.org/10.1021/acsphotonics.2c00828
ACS Photonics XXXX, XXX, XXX−XXX